ISSN 1063-7842, Technical Physics, 2020, Vol. 65, No. 11, pp. 1846–1852. © Pleiades Publishing, Ltd., 2020.
Russian Text © The Author(s), 2020, published in Zhurnal Tekhnicheskoi Fiziki, 2020, Vol. 90, No. 11, pp. 1931–1937.

PHYSICAL ELECTRONICS

Analysis of Electron Emission from a Single Silicon Cathode to Quasi-Vacuum (Air) Using Atomic Force Microscopy

I. D. Evsikov[a,*], S. V. Mit'ko[a], P. Yu. Glagolev[a], N. A. Djuzhev[a], and G. D. Demin[a]

[a] *National Research University MIET, Zelenograd, Moscow, 124498 Russia*

**e-mail: evsikov.ilija@yandex.ru*

Received April 16, 2020; revised April 16, 2020; accepted April 16, 2020

Abstract—Atomic force microscopy is employed in the experimental study of specific features of the field emission of electrons from a single silicon needle-type cathode to quasi-vacuum (air). Noncontact regime of the atomic force microscopy is used to measure the I–V characteristics of a single cathode with nanometer-scale tip radius at distances of 10 and 20 nm between the cathode tip and the measurement probe. Electric field distributions are simulated for both surface of the tip of a single cathode and tip surfaces of single cathodes in an array, and the results are used to theoretically estimate electric field enhancement versus cathode–probe distance. It is shown that the enhancement factor calculated from the experimental I–V characteristics in the Fowler–Nordheim coordinates is greater than the result of theoretical calculations by several orders of magnitude. This circumstance indicates that additional quantum dimensional effects that play an important role in the generation of the electron emission current in the nanoscale gap must be taken into account.

DOI: 10.1134/S1063784220110067

INTRODUCTION

There has been considerable recent interest in the development of vacuum nanoelectronic devices due to the fact that such devices exhibit stability against radiation, allow high-temperature working regimes, and provide high efficiencies in the THz range. Such positive features are related to physical properties of vacuum that provides ballistic transport of carriers (electrons) along the conduction channel almost in the absence of collisions. The phonon scattering of carriers by crystal lattice of semiconductors in the presence of current flow leads to undesired heating of the structure and formation of additional defects in the conduction channel. Such negative effects become critical on the 10-nm scale, which impedes further scaling down of semiconductor electronics [1]. Nevertheless, positive features of vacuum nanoelectronic devices (high efficiency and stability against radiation and high temperature) the working principle of which is based on field emission of electrons to vacuum can be combined with the positive features of the CMOS silicon technology (see the results of [2–4]). Moreover, such integration has been demonstrated in [5] in which novel combined devices have been based on conventional metal–oxide–semiconductor (MOS) transistor and vacuum FET with a conduction channel length of 100 nm and a operation voltage of 10 V. A further decrease in the operation voltage and, hence, power consumption and an increase in the life time of vacuum nanosized devices can be reached using a decrease in the length of the conduction channel [6–9]. However, note that the physical effects related to the field emission of electrons on the nanoscale, when the interelectrode gap is no greater than 20 nm, are insufficiently studied, which causes problems in precision designing of vacuum nanoelectronic devices [10]. In this work, the atomic force microscopy (AFM) is used to measure the I–V characteristics of single silicon cathodes the emission parameters of which are compared with the results of theoretical estimations based on simulation. Mean free path of electrons in air is about 68 nm, so that the study can be performed under quasi-vacuum conditions (in air) in the absence of an additional vacuum chamber, which substantially simplifies the experimental procedure. However, vacuum chamber is not needed for field-emission devices with a channel length of less than 20 nm, which provides compatibility with key procedures of the CMOS technology. Emission structures have been studied with the aid of AFM in [11, 12]. The AFM has been predominantly employed in the study of the surface structure. A distinctive feature of this work is related to the experimental study of the field emission of electrons from silicon nanosized cathodes at a sub-20-nm quasi-vacuum gap aimed at the analysis of specific features of the field-emission effects on such a scale. Note novelty of the study.

1. EXPERIMENTAL METHOD

AFM procedures were used in the study of the field emission of electrons from a single silicon cathode to

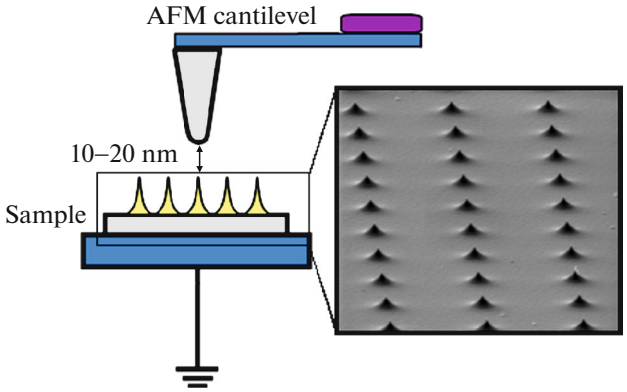

Fig. 1. Experimental scheme for the analysis of the field emission from a single field-emission cathode to quasi-vacuum (air) using the AFM.

quasi-vacuum (air) gap with a width of no greater than 20 nm (Fig. 1). The object under study is a fragment of an *n*-type silicon wafer with an array of field-emission needle-type cathodes that has been fabricated for application in X-ray lithography. Each cathode in the array provides fixed field-emission current needed for generation of the X-ray radiation in the predetermined region of the anode electrode with a through-type target responsible for formation of a single pixel of image on the X-ray resist [13]. A physical layout is successfully formed provided that the field-emission current is uniformly distributed over the target, and such a distribution is reached due to uniformity of the cathode sizes in the array. Carbon nanostructures (nanotubes, carbon monolayers (graphene), etc.) that exhibit high field-emission parameters do not satisfy the above requirement owing to specific features of synthesis, which determine relatively low reproducibility of sizes of single emitters in the array [14]. This circumstance leads to uncontrolled formation and burning out of emission centers and significant spread of the field-emission currents of emitters over the array [15]. Such a problem is also encountered in the technology for formation of the Spindt-type field-emission cathodes based on refractory metals (Au, W, and Mo) for which etching of metal layers is a complicated technological procedure that does not provide almost equal tip radii [16]. Exclusive advantages of the conventional silicon technology have been demonstrated in [17] for the formation of reproducible field-emission structures (minimum spread of cathode sizes in the array is reached, and current density of greater than 100 A/cm^2 can be obtained at a voltage of less than 75 V). Relatively high reproducibility of the technological process for fabrication of an array of silicon needle-type cathodes makes it possible to produce strictly periodic structures that are needed for devices in which high-density directional electron beams must be generated (in particular, systems of microfocus X-ray sources). The technological process of the formation of an array of silicon needle-type cathodes for the above applications has been presented in [13, 17]. A preliminary study of the samples with the aid of the scanning electron microscopy (SEM) has shown that the cathodes have nanoscale (about 10 nm) radius of the tip and a height of about 350 nm.

The I–V characteristic of a single silicon cathode from the array was measured with the aid of an AIST-NT SmartSPM-SPM 1000 atomic force microscope (Fig. 2). In the experiments, we used a K-TEK Nano DCP20 diamond-coated cantilever with a probe tip radius of 35 nm. Zero potential was provided for the measurement stage in the experiments. The I–V characteristics of single cathodes were measured in contact and noncontact regimes of surface scanning. AC voltage with the frequency that is close to oscillation frequency of the cantilever (about several tens of kilohertz) was fed to the cantilever of the atomic force microscope. Preliminary heating of the sample was not performed. A specific feature of the AFM measurements of the emission characteristics is related to the fact that the surface scanning can be performed at a distance of less than 20 nm from the tip of the selected cathode and the field emission can be initiated at atmospheric pressure. The mean free path of electrons in air is about 68 nm, so that the probability of electron collisions with molecules of gas medium is negligibly low at the specified distances (no greater than 20 nm) between the sample and measurement probe of the atomic force microscope [18]. Thus, we assume that air medium in the experiments is equivalent to vacuum.

2. EXPERIMENTAL RESULTS

Figure 3a presents the image of the scanned relief of a fragment of the sample with height scale. The field-emission cathodes can be identified using bright periodic spots on the image. Figure 3b shows the 3D image of a fragment of the needle-type-cathode array that is obtained in the noncontact scanning regime of the atomic force microscope. Two main parameters (field enhancement factor β and effective emission area S_{eff}) characterize the efficiency of field-emission cathodes. It is known that the emission current of the field-emission cathode directly depends on local electric field E_S on the surface of the tip. Normally, local field E_S is greater than macroscopic field E_m of the plane-parallel configuration of electrodes. The ratio of such fields is the field-enhancement factor [19]:

$$\beta = \frac{E_S}{E_m} = E_S \frac{d}{U}, \quad (1)$$

where d is the distance between the cathode and the measurement probe and U is the interelectrode voltage (between tip of cathode and probe of cantilever).

For a perfect configuration of the emitter, uniform local electric field E_S on the emitter surface, and uni-

Fig. 2. Photograph of the SMART-SPM 1000 atomic force microscope that was used in the experiments.

form work function φ, effective emission area is formally represented as $S_{\text{eff}} = I_{\text{fe}}/j_{\text{fe}}$, where I_{fe} is the full emission current of the cathode and j_{fe} is emission current density. For a nonuniform distribution of the field over the cathode surface, the full current from the emitter is calculated using integration of current density over the surface: $I_{\text{fe}} = \int j_{\text{fe}}(E_S)dS$. In the experimental study of real cathode–anode systems, it is expedient to determine the above parameters (β and S_{eff}) using the analysis of the I–V characteristics of the emission structure plotted on semilogarithmic Fowler–Nordheim coordinates and approximated using a linear dependence. The parameters are related to slope K and intercept R of trend line that can be obtained from the field-emission equation reduced to macroscopic current I_{fe} and voltage U [20]:

$$I_{\text{fe}} = S_{\text{eff}} A \left(\frac{\beta U}{d\varphi^{1/2}}\right)^2 \exp\left(-\frac{Bd\varphi^{3/2}}{\beta U}\right), \qquad (2)$$

where φ is the work function of cathode material, $A = 1.54 \times 10^{-6}$ [A eV V^{-2}] is the first Fowler–Nordheim constant, and $B = 6.83 \times 10^9$ [eV$^{-3/2}$ V m^{-1}] is the second constant. On the Fowler–Nordheim coordinates, Eq. (2) is represented as

$$\ln\left(\frac{I_{\text{fe}}}{U^2}\right) = \ln\left(\frac{AS_{\text{eff}}\beta^2}{d^2\varphi}\right) - \frac{Bd\varphi^{3/2}}{\beta U} = R + \frac{K}{U}. \qquad (3)$$

In accordance with Eq. (3), the effective parameters of the emitter are calculated as

$$\beta = \frac{Bd}{K}, \quad S_{\text{eff}} = \frac{\exp(R)d^2}{A\beta^2}. \qquad (4)$$

Figure 4 presents three types of the I–V characteristics of a single silicon cathode for cantilever voltages ranging from −10 to 10 V. The characteristics were obtained for both noncontact (d = 10 and 20 nm (Figs. 4a, and 4b, respectively)) and contact (Fig. 4c) scanning regimes. Variations in the voltage were repeated five times in the absence of long time intervals between scannings. The insets to Fig. 4 show the

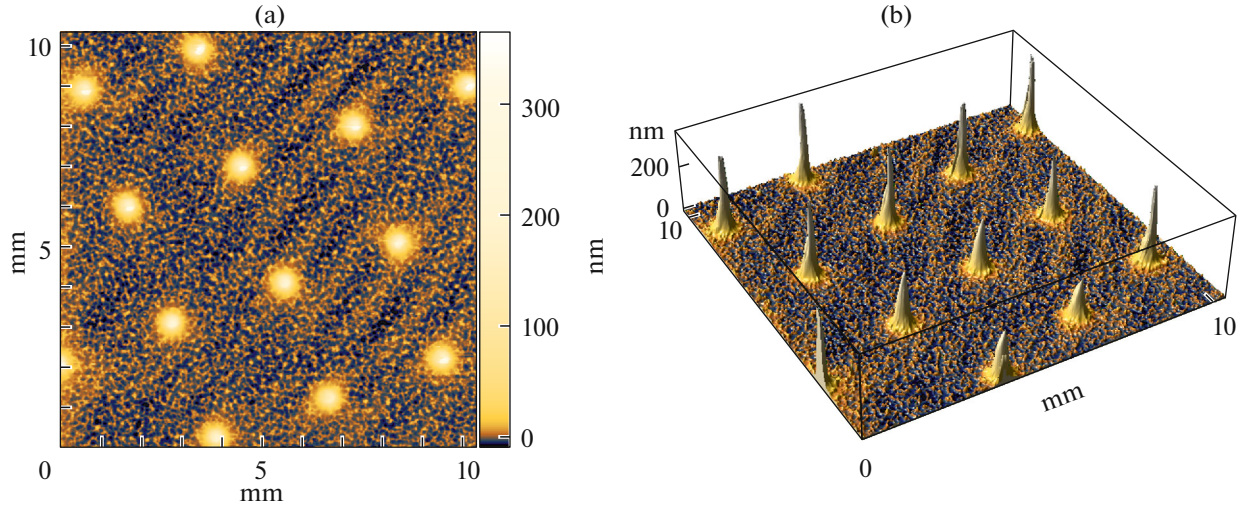

Fig. 3. (a) AFM image of a fragment of the array of silicon cathodes (top view) and (b) 3D model of the fragment of the array of silicon cathodes obtained using the AFM.

Table 1. Effective parameters of a single silicon cathode for two distances between the cathode and measurement probe

Cathode–probe distance, nm	β, deg	S_{eff}, μm^2
10	55.5	0.318
20	103.8	0.343

experimental and linear approximating I–V characteristics of the field-emission cathode plotted on the Fowler–Nordheim coordinates for cathode–probe distances of 10 and 20 nm. The I–V characteristics are presented on the Fowler–Nordheim coordinates for voltage ranging from 5 to 10 V when the cathode current is greater than 1 nA (region of stable field emission). The curves that approximate the I–V characteristics on conventional coordinates for cathode–probe distances of 10 and 20 nm can be represented as a sum of exponential functions: $I_{fe}(U) = a_1\exp(b_1U) - a_2\exp(-b_2U)$, where the approximation coefficients are $a_1 = 9.754 \times 10^{-2}$, $b_1 = 4.719 \times 10^{-1}$, $a_2 = 1.317 \times 10^{-1}$, and $b_2 = 3.599 \times 10^{-1}$ for the I–V characteristic of Fig. 4a ($d = 10$ nm) and $a_1 = 8.469 \times 10^{-2}$, $b_1 = 4.7 \times 10^{-1}$, $a_2 = 1.343 \times 10^{-1}$, and $b_2 = 3.279 \times 10^{-1}$ for the I–V characteristic of Fig. 4b ($d = 20$ nm). For Figs. 4a and 4b, the shapes of the approximating curves $I_{fe}(U)$ are determined by the fact that the I–V characteristics for cathode–probe distances of 10 and 20 nm can be divided into two regions (with positive $U > 0$ and negative $U < 0$ voltages of the cantilever of the atomic force microscope). At $U > 0$, the field emission of electrons takes place from a single silicon cathode to the measurement probe of the microscope. At $U < 0$ electrons are emitted from the measurement probe to the cathode. Note that the emission properties of the cantilever probe differ from the emission properties of the silicon cathode, which accounts for asymmetric character of the I–V characteristics relative to zero. The curve that approximates the I–V characteristics on conventional coordinates for the contact regime (Fig. 4c) represents the sextic polynomial $I_{fe} = f(U) = \sum_{i=0\ldots6} C_i U^i$, where $C_0 = -3.633$, $C_1 = -1.071$, $C_2 = 1.316$, $C_3 = 4.789 \times 10^{-1}$, $C_4 = 3.206 \times 10^{-2}$, $C_5 = -2.348 \times 10^{-4}$, and $C_6 = -2.32 \times 10^{-4}$. Determination coefficients R^2, which characterize the reliability of approximation of the I–V characteristics plotted on conventional coordinates are $R^2 = 0.9636$ (Fig. 4a), $R^2 = 0.9661$ (Fig. 4b), and $R^2 = 0.9966$ (Fig. 4c). The linear dependence that approximates the experimental I–V characteristics plotted on the Fowler–Nordheim coordinates is given by $\ln(I_{fe}/U^2) = a + b/U$, where $a = -1.175$ and $b = -11.75$ (inset to Fig. 4a) and $a = -1.231$ and $b = -12.56$ (inset to Fig. 4b). The determination coefficients are $R^2 = 0.8278$ (Fig. 4a) and $R^2 = 0.7969$ (Fig. 4b). Table 1 presents the effective emission parameters of a single silicon cathode calculated with the aid of formula (4) for distances of $d = 10$ and 20 nm, which were used in the experiments. It is seen that field enhancement factor β proportionally increases with the distance from the probe to the cathode under study. The calculations show that emission area $\mathbf{S}_{eff}$ slightly increases (by 8%) with an increase in the cathode–probe distance.

3. MODEL AND MAIN EQUATIONS

For comparison of the experimental and theoretical results, we employed the finite-element method to numerically simulate the electric field distribution over the surface of the silicon cathode that was studied with the aid of AFM. For this purpose, the COMSOL MultiPhysics software package [21] was used to construct two 3D models that simulate the experiment and represent the following systems: ((i) single cathode and measurement probe and (ii) array of cathodes and measurement probe. The SEM and AFM results for the samples under study were used to determine geometrical parameters of the cathodes (height, tip radius, and shape of the cathode surface).

The Electrostatics physicomathematical module from the COMSOL MultiPhysics software package was used to calculate the electric field distribution over the surface of the tip of a single silicon cathode and surfaces of tips of cathodes in the array. The electric field $\mathbf{E} = -\nabla\phi$ was calculated using the solution to the Poisson equation

$$-\nabla \cdot (\nabla\phi) = \frac{\rho}{\varepsilon_0}, \quad (5)$$

where $\phi = \phi(\mathbf{r})$ is the potential at arbitrary point $\mathbf{r} = (x, y, z)$ of the system, ρ is the volume charge density, and $\varepsilon_0 = 8.85 \times 10^{-12}$ [F m^{-1}] is the permittivity of vacuum. With allowance for the dielectric properties of material, Eq. (5) is generally represented as $\nabla \cdot (\varepsilon_0\varepsilon_r\mathbf{E})$, where ε_r is the third-rank tensor of permittivity. Field enhancement factor β for the cathode tip was calculated using formula (1).

4. SIMULATED RESULTS

Figure 5 illustrates the simulated electric field distribution for the surface of the tip of a single silicon cathode for the experimental parameters ($d = 10$ nm and $U = 10$ V). The inset shows variations in factor β along line L (intersection of a vertical plane and cathode surface). It is seen that field enhancement factor exponentially decreases with an increase in the distance from the tip of the silicon emitter. For a distance of $d = 10$ nm, the calculated field enhancement factor on the tip of single cathode (about 2.25) is less than the factor obtained from the experimental I–V characteristics of a single cathode by an order of magnitude. Such a result can be due to shape changes (extension of fragments) of the surface of the silicon emitter in the

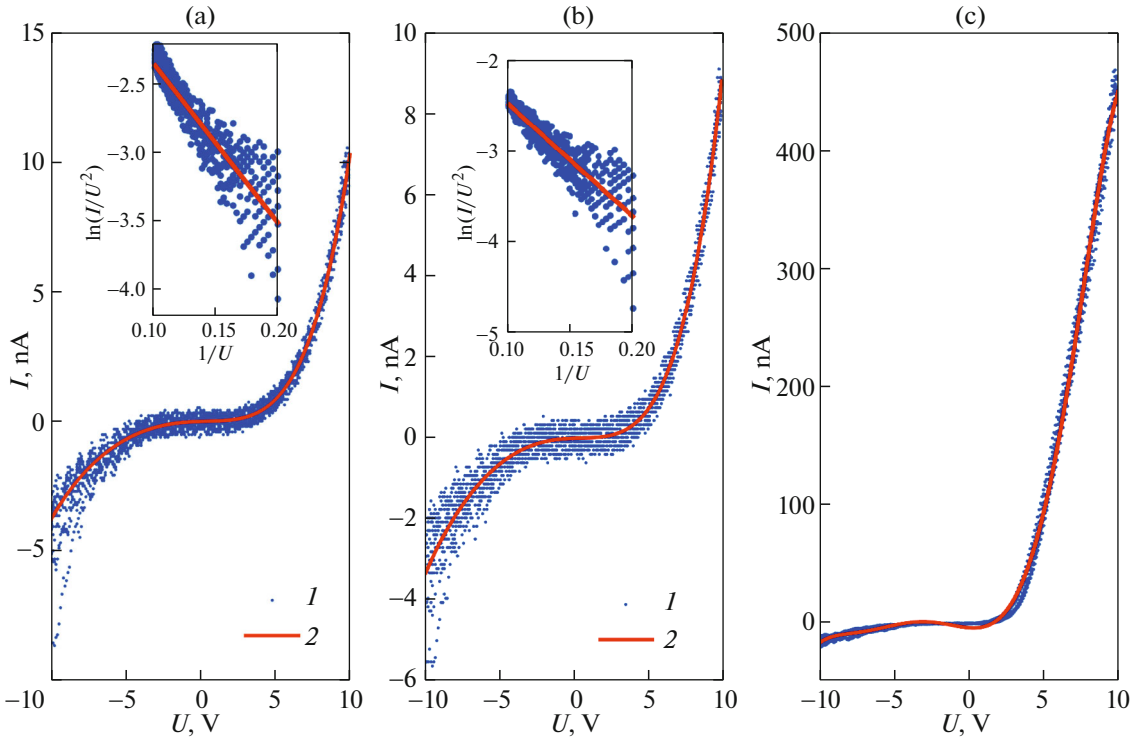

Fig. 4. *I–V* characteristics of a single silicon cathode on conventional and (inset) Fowler–Nordheim coordinates at cathode–probe distances of (a) 10, (b) 20, and (c) 0 nm (contact): (*1*) experimental and (*2*) approximating curves.

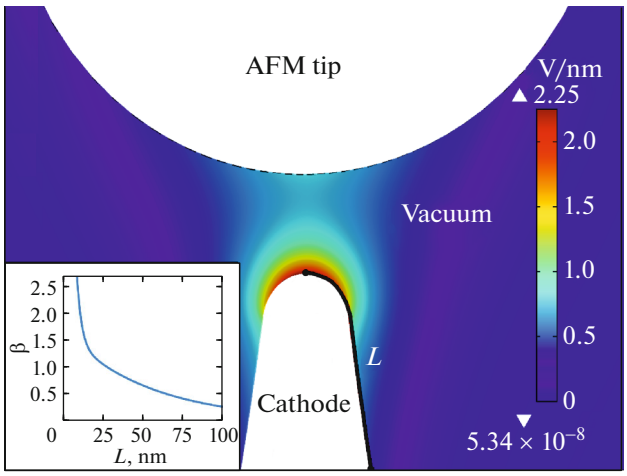

Fig. 5. Electric field distribution in the system consisting of a single cathode and the measurement probe of cantilever for a fixed cathode–probe distance of $d = 10$ nm and a voltage of $U = 10$ V. The inset shows variations in the electric field amplitude along line L (intersection of cathode surface and vertical plane) versus distance from the tip.

presence of a relatively strong electric field in the nanometer-size gap, which have been observed in [22] at cathode–probe distances of several hundreds of nanometers. Such an effect can be due to distortion of the potential barrier at the silicon–vacuum interface that depends on the radius of curvature of the surface

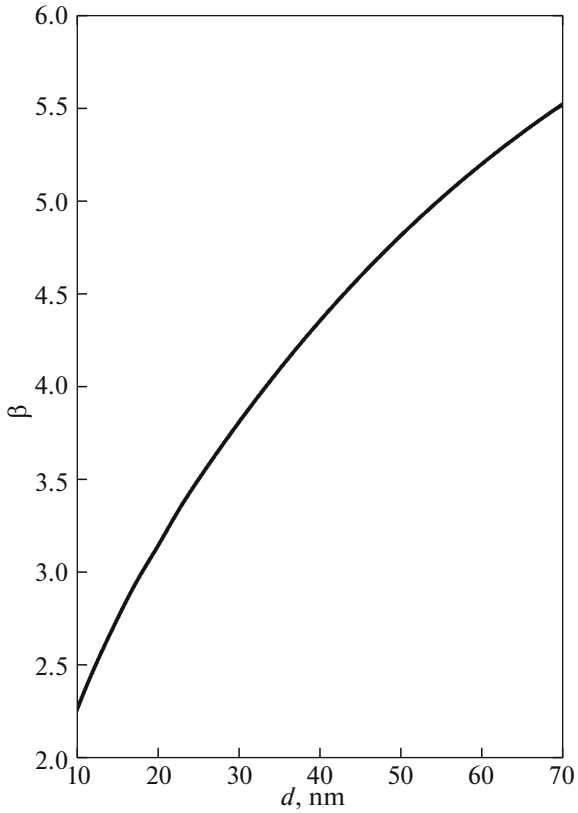

Fig. 6. Plot of field enhancement factor β on the tip of a single silicon cathode vs. cathode–probe distance *d*.

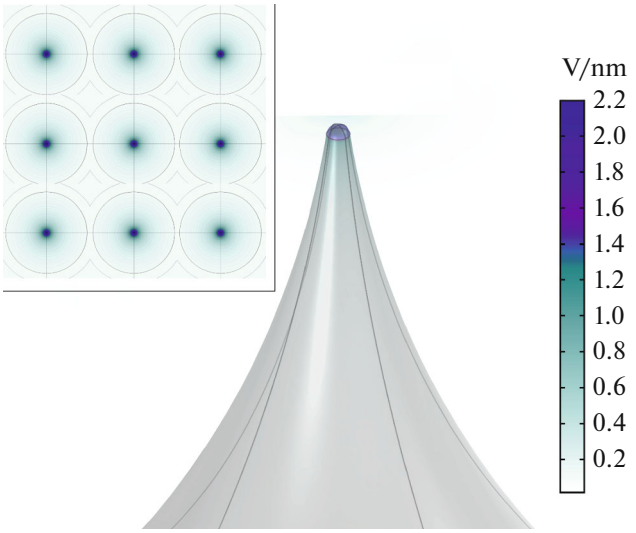

Fig. 7. Electric field distribution in the system consisting of a 3 × 3 array of cathodes and the measurement probe of cantilever for distance $d = 10$ nm and applied voltage $U = 10$ V. The inset shows the electric field distribution for the array (top view).

of the silicon emitter [23, 24] and, hence, variations in factor β and field-emission current. This circumstance can be used to interpret the above difference with the experimental results and must be taken into account in the simulation. Figure 6 shows the dependence of field enhancement factor β on the cathode–probe distance that ranges from 10 to 70 nm (corresponds to mean free path of electrons in air). It is seen that factor β gradually increases with distance d, which is in agreement with the experimental results and related to faster decrease in macroscopic field $E_m = U/d$ relative to a decrease in local field E_S on the tip. Dependence $\beta = f(d)$ is perfectly (determination coefficient is $R^2 = 1$) approximated using the analytical function $\beta = b_0 + b_1 d + b_2/d + b_3/d^2$, where $b_0 = 2.074$, $b_1 = 0.07383$, $b_2 = -5.362$, and $b_3 = -3.349 \times 10^{-4}$. For the 3 × 3 cathode array, the simulated electric field is uniformly distributed over the cathode tips (Fig. 7) and the numerical values are in agreement with those for a single silicon cathode. The intercathode distance in the experimental array is about 3 μm, so that the neighborhood of the cathode selected by the probe insignificantly affects the electric field on its surface.

CONCLUSIONS

We have considered a method for analysis of the field emission from a single silicon cathode in air (quasi-vacuum) on the nanoscale. The AFM method has been used to obtain the I–V characteristics of a single cathode in a cathode array that make it possible to determine specific features of the field emission for the corresponding length of the quasi-vacuum conduction channel (10 or 20 nm). Effective emission parameters (field enhancement factor β and emission area S_{eff}) have been calculated for each case. To interpret the experimental results, we have simulated the electric field of the system under study (sample and AFM probe) in which a single needle-type cathode or a 3 × 3 array of cathodes serves as the sample. The analysis of the results shows that additional effects in the vicinity of the emitter surface must be taken into account (in particular, distortions of the potential barrier due to probable deformation of the near-surface region of the emitter in the presence of a strong electric field in the nanosized gap). Such effects may serve as a reason for the difference of the theoretically calculated and experimental field enhancement factors. The results of this work can be used in the correct theoretical analysis of the field emission of electrons from semiconductor emitters on nanoscale, which is beyond the framework of the classical Fowler–Nordheim theory.

FUNDING

This work was supported by the RF Presidential grant no. 075-15-2019-1139.

ACKNOWLEDGMENTS

We are grateful to the RF Ministry of Education and Science for technical support provided by the MIET Core facilities center "MEMS and electronic components."

CONFLICT OF INTERESTS

The authors declare that there is no conflicts of interest.

REFERENCES

1. K. Seshan, in *Handbook of Thin Film Deposition* (Elsevier, 2018), pp. 19–41. https://doi.org/10.1016/B978-0-12-812311-9.00002-5
2. S. Nirantar, T. Ahmed, M. Bhaskaran, J.-W. Han, S. Walia, and S. Sriram, Adv. Intell. Syst. **1** (4), 1900039 (2019). https://doi.org/10.1002/aisy.201900039
3. J.-W. Han, D.-I. Moon, and M. Meyyappan, Nano Lett. **17**, 2146 (2017). https://doi.org/10.1021/acs.nanolett.6b04363
4. J.-W. Han, M.-L. Seol, D.-L. Moon, G. Hunter, and M. Meyyappan, Nat. Electron. **2**, 405 (2019). https://doi.org/10.1038/s41928-019-0289-z
5. J.-W. Han, J. S. Oh, and M. Meyyappan, IEEE Trans. Nanotechnol. **13**, 464 (2014). https://doi.org/10.1109/TNANO.2014.2310774
6. S. Nirantar, T. Ahmed, G. Ren, P. Gutruf, C. Xu, M. Bhaskaran, S. Walia, and S. Sriram, Nano Lett. **18**, 7478 (2018). https://doi.org/10.1021/acs.nanolett.8b02849

7. J. Xu, Q. Wang, Z. Tao, Y. Zhai, C. Guangdian, Z. Qi, and X. Zhang, IEEE Trans. Electron Devices **64**, 2364 (2017). https://doi.org/10.1109/TED.2017.2673853
8. J. Xu, H. Hu, W. Yang, C. Li, Y. Shi, Y. Shi, Q. Wang, and X. Zhang, Nanotechnology **31**, 065202 (2020). https://doi.org/10.1088/1361-6528/ab51cb
9. M. Liu, W. Fu, Y. Yang, T. Li, and Y. Wang, Appl. Phys. Lett. **112**, 093104 (2018). https://doi.org/10.1063/1.4996370
10. W.-T. Chang, H.-J. Hsu, and P.-H. Pao, Micromachines **10** (12), 858 (2019). https://doi.org/10.3390/mi10120858
11. V. Chatterjee, R. Harniman, P. W. May, and P. K. Barhai, Appl. Phys. Lett. **104**, 171907 (2014). https://doi.org/10.1063/1.4875059
12. R. V. Konakova, O. B. Okhrimenko, A. M. Svetlichnyi, O. A. Ageev, E. Yu. Volkov, A. S. Kolomiytsev, I. L. Jityaev, and O. B. Spiridonov, Semiconductors **49** (9), 1242 (2015). https://doi.org/10.1134/S1063782615090146
13. N. A. Djuzhev, G. D. Demin, N. A. Filippov, I. D. Evsikov, P. Yu. Glagolev, M. A. Makhiboroda, N. I. Chkhalo, N. N. Salashchenko, S. V. Filippov, A. G. Kolosko, E. O. Popov, and V. A. Bespalov, Tech. Phys. **64** (12), 1742 (2019). https://doi.org/10.1134/S1063784219120053
14. S. M. Jung, J. Hahn, H. Y. Jung, and J. S. Suh, Nano Lett. **6**, 1569 (2006). https://doi.org/10.1021/nl060437q
15. N. Zhu and J. Chen, Micromachines **8**, 162 (2017). https://doi.org/10.3390/mi8050162
16. S. A. Guerrera and A. I. Akinwande, Nanotechnology **27**, 295302 (2016). https://doi.org/10.1088/0957-4484/27/29/295302
17. G. D. Demin, N. A. Djuzhev, N. A. Filippov, P. Yu. Glagolev, I. D. Evsikov, and N. N. Patyukov, J. Vac. Sci. Technol., B **37**, 022903 (2019). https://doi.org/10.1116/1.5068688
18. L. Qian, Y. Wang, L. Liu, and S. Fan, J. Vac. Sci. Technol., B **28**, 562 (2010). https://doi.org/10.1116/1.3372333
19. R. G. Forbes, C. J. Edgcombe, and U. Valdré, Ultramicroscopy **95**, 57 (2003). https://doi.org/10.1016/s0304-3991(02)00297-8
20. E. O. Popov, A. G. Kolosko, M. A. Chumak, and S. V. Filippov, Tech. Phys. **64** (10), 1530 (2019). https://doi.org/10.1134/S1063784219100177
21. *COMSOL Multiphysics. V. 5.5. COMSOL AB* (Stockholm, Sweden), https://www.comsol.com.
22. H. D. Nguyen, J. S. Kang, M. Li, and Y. Hu, Nanoscale **11**, 3129 (2019). https://doi.org/10.1039/c8nr07912a
23. Y. Huang, Z. Deng, W. Wang, C. Liang, J. She, S. Deng, and N. Xu, Sci. Rep. **5**, 10631 (2015). https://doi.org/10.1038/srep10631
24. J. A. Driscoll, S. Bubin, W. R. French, and K. Varga, Nanotechnology **22**, 285702 (2011). https://doi.org/10.1088/0957-4484/22/28/285702

Translated by A. Chikishev